Research Article
Volume 12:1, 2025

Journal of Lasers, Optics & Photonics

ISSN: 2469-410X Open Access

# Crystal Growth, Characterization and Theoretical Insights of an Organic Schiff base 2-(1-(2,4 Dichlorophenyl)Ethylidene)Hydrazine Carboxamide for NLO Applications

**N. Sudha[1], R. Ananthi[1*], M. Sowmiya[1], R. Rajesh Kanna[2]**

*[1]PG and Research Department of Physics, Sri Sarada College for Women (Autonomous) Salem-16, Tamilnadu, India*

*[2]Department of Electronics and Communication Engineering, Chennai Institute of Technology, Kundrathur, Chennai-600069, India*

## Abstract

Organic crystals semicarbazone of 2,4-dichloroacetophenone (Chemical name 2-(1-(2,4 dichlorophenyl)ethylidene)hydrazine carboxamide) DCAP has been grown by slow evaporation method. The structure is confirmed by single XRD. Quantum chemical calculations of geometric structure, vibrational analysis and VCD of the title compound are carried out by DFT method with 6-31+G (d,p) basis set. Both the experimental and theoretical vibrational spectra confirm the presence of functional groups. Hirshfeld surface analysis provides relevant information about the intermolecular interactions of the molecules. Optical properties have been obtained from UV-vis and photoluminescence spectral analyses. Kurtz and Perry method is used to test the frequency conversion property of DCAP crystal. Hardness and dielectric studies are carried out to understand the strength of the crystal. HOMO-LUMO and MESP energies confirm the chemical reactivity of the molecule. Thermal properties are obtained by TG/DTA analysis. Hyper polarizability calculations also confirm its nonlinearity.

**Keywords:** Crystal growth • Quantum chemical calculations • NLO property

## Introduction

The properties and performance of nonlinear optical and photonic materials depend critically on their composition, microstructure and purity. Convection and sedimentation can cause variations in processing conditions of such materials, which in turn, can affect the morphology and microstructure of the materials and thereby, also the optical properties [1,2]. The large nonlinear optical effect found in some organic crystals make the materials attractive for applications in frequency conversion [3]. Optoelectronics and NLO are expected to play a major role in photonics which is emerging as frontier areas of science and technology. The organic molecular materials have emerged as a new class of promising nonlinear optical materials because of their superior qualities over inorganic systems. Among the nonlinear phenomena frequency doubling, frequency mixing and electro-optic modulation are important in the fields of optical image storage and optical communications [4-6]. Crystal growth from solution is a powerful purification process and the purity of the obtained crystals is higher than the corresponding starting reactants. Also, the low temperature solution growth makes it easier to obtain less defective crystals than in high temperature growth methods [7]. The single crystal structure has been solved by Hoong-Kun Fun, et al. To the best of our knowledge so far, no systematic study has been carried out on the vibrational, thermal, linear and nonlinear optical properties of the title crystal. Hence our present intention is to provide a complete study of this material with respect to its physico-chemical properties. The grown crystals have been subjected to experimental characterizations and theoretical calculations to confirm its nonlinearity.

## Materials and Methods

### Experimental details

1 mmol of 2, 4 dichloroacetophenone is mixed with 2 mmol semicarbazide hydrochloride and 3 mmol of anhydrous sodium acetate in 10 ml of ethanol. The mixture is refluxed for 4 hours. A white precipitate is obtained and washed with water. The reaction scheme is shown in Figure 1. This precipitate is recrystallized using methanol as solvent repeatedly to obtain transparent needle shaped

***Address for Correspondence:** R Ananthi, PG and Research Department of Physics, Sri Sarada College for Women (Autonomous) Salem-16, Tamilnadu, India; E-mail: ananthigk12@gmail.com*



**Received:** 06 April, 2024, Manuscript No. JLOP-24-131683; **Editor assigned:** 09 April, 2024, PreQC No. JLOP-24-131683 (PQ); **Reviewed:** 23 April, 2024, QC No. JLOP-24-131683; **Revised:** 01 July, 2025, Manuscript No. JLOP-24-131683 (R); **Published:** 28 July, 2025, DOI: 10.37421/2469-410X. 2025.12.180

crystals of semicarbazone of 2,4-dichloroacetophenone (chemical name 2-(1-(2,4 dichlorophenyl)ethylidene)hydrazine carboxamide) as shown in Figure 2.

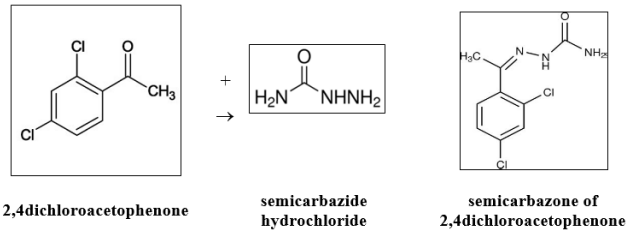


**Figure 1.** Reaction scheme of DCAP.

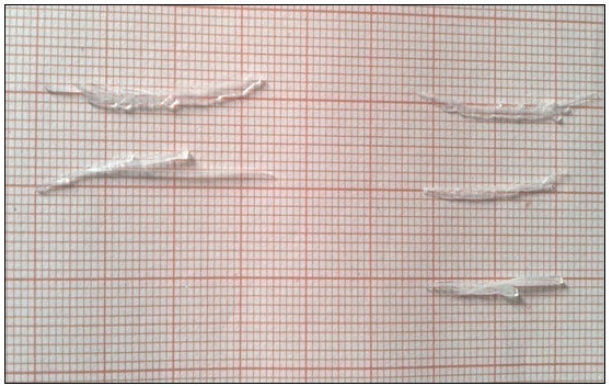

**Figure 2.** As grown crystals of DCAP.

### Computational details

Density functional theory is a phenomenally successful approach to find the solutions of the fundamental equation that describes the structural properties of atoms and molecules. All calculations are carried out with aid of Gaussian 09 package [8] with the help of three-parameter hybrid functional (B3) for the exchange part and Lee-Yang-Parr (LYP) correlation function, using 6-31+G(d,p) basis set [9]. An empirical uniform scaling factor of 0.956 is used to neglect the electron correlation and vibrational anharmonic [10]. The scaled frequencies were deviated <10 $cm^{-1}$ with few exceptions from the experimental frequencies. Furthermore, the dipole moment, linear polarizability, hyperpolarizability, frontier molecular orbital energies, VCD spectrum of DCAP were calculated at B3LYP/6-31+G(d,p) level. Molecular Hirshfeld surfaces calculations were performed using Crystal Explorer program.

## Results and Discussion

### Crystal structure analysis and molecular geometry

The DCAP crystal structure belongs to the monoclinic system with the space group C2/c. The lattice parameters are a=37.8079 (17) A, b=3.8097 (2) A,c=14.4920 A, β=98.852°. The cell volume is 2062.52 (17) $A^3$ containing Z=8 formula units. The asymmetric unit consists the semicarbazone group (C9/C6/C7/N1/N2/C8/O1/N3) is approximately planar with an r.m.s bond length deviation of 0.011 (2) Å for atom N1, while the dihedral angle between the least-squares plane through the semicarbazone group and the benzene ring is 38.76 (9)°. The thermal displacement ellipsoid plot with 50% probability level and optimised structure are presented in Figure 3 and Figure 4 respectively. The molecules are linked *via* N-H...O hydrogen bonds to generate R2 2(8) ring motifs. These motifs are further connected through C-H...O hydrogen bonds to form a one-dimensional chain along the (0 1 0) direction is shown in Figure 5. The complete structure details are shown in Table 1. H atoms are positioned geometrically (C-H=0.93–0.96 Å) and refined using a riding model with U iso(H)=1.2 Ueq(C) and 1.5 Ueq(methyl C). A rotating–group model is used for the methyl groups. The nitrogen H atoms are located from the difference Fourier map (N–H=0.85(3)–0.91(3) Å) and allowed to refine freely (Figure 5) [11].

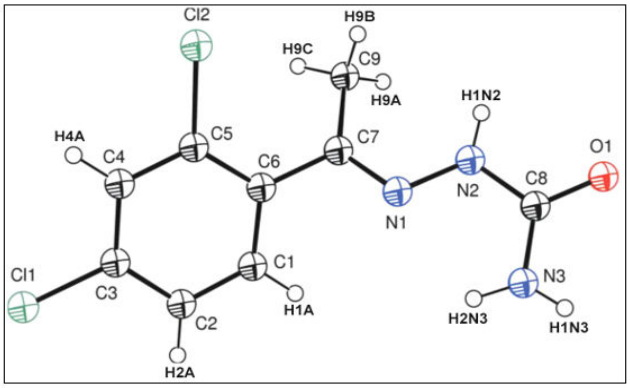


**Figure 3.** Ortep diagram of DCAP with atomic numbering scheme.

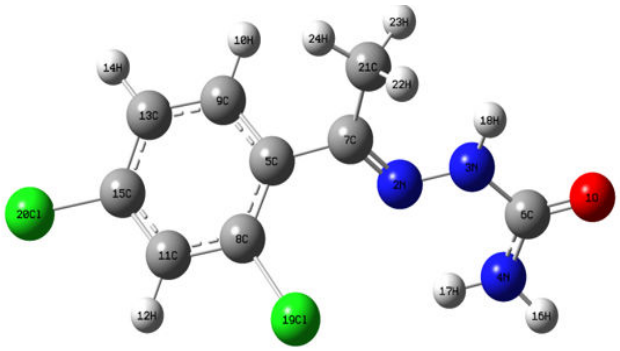

**Figure 4.** Optimized molecular structure of DCAP.

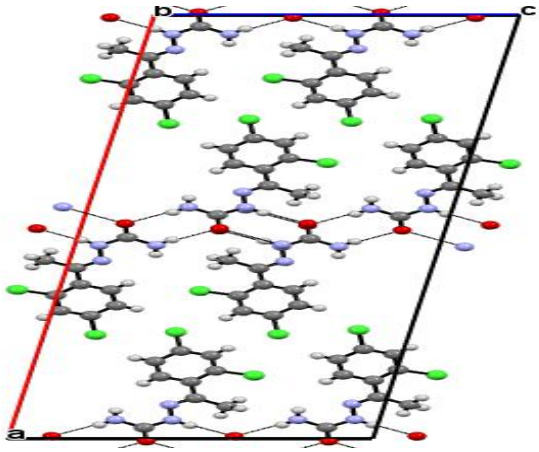


**Figure 5.** Packing diagram of DCAP along b axis.

| **Identification code** | **DCAP** |
|---|---|
| Empirical formula | $C_9H_9Cl_2N_3O$ |
| Formula weight | 246.09 |
| Temperature | 100 K |
| Wavelength | 0.7107 Å |
| Crystal system | Monoclinic, |
| Space group | C2/c |
| Unit cell dimensions | a=37.8079 (17) A, b=3.8097 (2) A, β=98.852 (2)°, c=14.4920 (7) A |
| Volume | 2062.52 (17) $A^3$ |
| Z | 8 |
| Density (calculated) | 1.585 $Mg/m^3$ |
| Absorption coefficient | 0.60 $mm^{-1}$ |
| F(000) | 1008 |
| Crystal size | 0.42 × 0.14 × 0.04 $mm^3$ |
| Theta range for data collection | 2.9-34.0° |
| Index ranges | -59<=h<=58, -5<=k<=5, -22<=l<=22 |
| Reflections collected | 32124 |
| Independent reflections | 4202 (R(int)=0.037) |
| Completeness to theta=24.991° | 98.40% |
| Absorption correction | Semi-empirical from equivalents |
| Max. and min. transmission | 0.974 and 0.707 |
| Refinement method | Full-matrix least-squares on $F^2$ |
| Data/restraints/parameters | 3559 / 30 / 325 |
| Goodness-of-fit on $F^2$ | 1.027 |
| Final R indices (I>2sigma(I)) | R1=0.0802, wR2=0.1974 |
| R indices (all data) | R1=0.0986, wR2=0.2086 |
| Absolute structure parameter | 0.0 (10) |
| Extinction coefficient | n/a |
| Largest diff. peak and hole | 0.409 and -0.302 e.$Å^{-3}$ |

**Table 1.** Crystal data and structure refinement details of DCAP crystal.

The compound is shaped by blending of 2,4-dichloroacetophenone with semicarbazide hydrochloride and due to conjugation of C=N, a Schiff base semicarbazone of 2,4-dicholoroacetophenone is formed. The compound contains a benzene ring in which the chain is substituted in ortho position. Here the formation of C=N are significant in making a non-centro symmetry structure of the molecules leading to nonlinear optical property [12]. 2,4-dichloroacetophenone is an aromatic cyclic compound which possesses number of hydrogen bonds with high degree of symmetry. The C=O at para position in phenyl ring gained higher order symmetry by the π-bond delocalization electron clouds which leads the compound to have second order of polarization and hyper polarizability. This is the main root cause to attain NLO properties when the compound is brought to crystal form [13]. The bond length C6-C7 of the chain is found to be 1.489 Å which is 0.099 Å greater than the C-C of the ring. This bond length is stretched out due to the maintaining of repulsive force between the charge clouds of the chain and ring. The bond length C8-N3 is 0.048 Å greater than C7-N1 due to the π and σ bond interactions respectively [14]. The observed value of the bond length C=O is found to be 1.23 Å however the title compound shows 1.256 Å for C=O. This is mainly due to the further substitution of $NH_2$ group on C [15]. Usually, the bond length of C=N is 1.287 Å [16]. Where as in the grown crystal bond length is 1.369 Å which is extend by 0.081 Å due to link of azine (N-N) group. The general value of N-N bond length is 1.47 Å but in the present case the bond length has reduced to 1.37 because of steeving of the ketone group with in the chain. However, there is not much change in C-Cl bond length as it coincides with the actual value 1.78. The bond length for C8-N2 (1.369 A) is greater than the bond length of C7-N1 which is due to the attachment of $NH_2$ and =O (electronegative groups) in the crystal structure. The observed C8–O1 bond length is higher than the theoretical value. Similarly, the N2-C8 and N3-C8 bond lengths are lesser than theoretical values. All these can be explained because of resonance involving lone pair on the nitrogen atoms. The experimental structural bond lengths and bond angles from XRD and computed optimized counterparts are tabulated in Tables 2. and 3. respectively. The small differences which originate from the theoretical calculation is due to the isolated molecule in gas phase.

| Atoms with numbering | Experimental bond length (Å) | Theoretical bond length (Å) | Atoms with numbering | Experimental bond length (Å) | Theoretical bond length (Å) |
|---|---|---|---|---|---|
| Cl1-C3 | 1.74 | 1.754 | C1-H1A | 0.93 | 1.085 |
| Cl2-C5 | 1.74 | 1.757 | C2-C3 | 1.39 | 1.394 |
| O1-C8 | 1.25 | 1.226 | C2-H2A | 0.93 | 1.083 |
| N1-C7 | 1.29 | 1.289 | C3-C4 | 1.38 | 1.392 |
| N1-N2 | 1.37 | 1.352 | C4-C5 | 1.39 | 1.397 |
| N2-C8 | 1.36 | 1.398 | C4-H4A | 0.93 | 1.083 |
| N2-H1N2 | 0.85 | 1.014 | C5-C6 | 1.39 | 1.408 |
| N3-C8 | 1.33 | 1.36 | C6-C7 | 1.48 | 1.488 |
| N3-H1N3 | 0.88 | 1.006 | C7-C9 | 1.5 | 1.513 |
| N3-H2N3 | 0.81 | 1.009 | C9-H9A | 0.96 | 1.09 |
| C1-C2 | 1.39 | 1.391 | C9-H9B | 0.96 | 1.098 |
| C1-C6 | 1.39 | 1.407 | C9-H9C | 0.96 | 1.098 |

**Table 2.** Comparison of experimental and calculated bond lengths of DCAP crystal.

| Atoms with numbering | Experimental bond angle (deg) | Theoretical bond angle (deg) | Atoms with numbering | Experimental bond angle (deg) | Theoretical bond angle (deg) |
|---|---|---|---|---|---|
| C7-N1-N2 | 117.12 | 119.459 | C4-C5-C6 | 122.38 | 121.707 |
| C8-N2-N1 | 118.08 | 121.546 | C4-C5-C12 | 116.02 | 116.334 |
| C8-N2-H1N2 | 113 | 114.945 | C6-C5-C12 | 121.59 | 121.919 |

| | | | | | |
|---|---|---|---|---|---|
| N1-N2- H1N2 | 128 | 123.507 | C5-C6-C1 | 116.83 | 116.737 |
| C8-N3-H1N3 | 115 | 117.167 | C5-C6-C7 | 123.95 | 124.572 |
| C8-N3-H2N3 | 112 | 120.361 | C1-C6-C7 | 119.21 | 118.692 |
| H1N3-N3-H2N3 | 131 | 120.857 | N1-C7-C6 | 114.76 | 116.988 |
| C2-C1-C6 | 122.24 | 122.657 | N1-C7-C9 | 124.43 | 123.471 |
| C2-C1-H1A | 118.9 | 118.637 | C6-C7-C9 | 120.65 | 119.53 |
| C6-C1-H1A | 118.9 | 118.692 | O1-C8-N3 | 122.71 | 125.253 |
| C3-C2-C1 | 118.53 | 118.629 | O1-C8-N2 | 120.16 | 119.693 |
| C3-C2-H2A | 120.7 | 120.522 | N3-C8-N2 | 117.11 | 115.048 |
| C1-C2-H2A | 120.7 | 120.848 | C7-C9-H9A | 109.5 | 110.404 |
| C4-C3-C2 | 121.52 | 120.921 | C7-C9-H9B | 109.5 | 111.774 |
| C4-C3-C11 | 118.62 | 119.265 | H9A-C9-H9B | 109.5 | 107.487 |
| C2-C3-C11 | 119.83 | 119.813 | C7-C9H-9C | 109.5 | 111.529 |
| C3-C4-C5 | 118.48 | 119.338 | H9A-C9-H9C | 109.5 | 107.291 |
| C3-C4-H4A | 120.8 | 120.638 | H9B-C9-H9C | 109.5 | 108.158 |
| C5-C4-H4A | 120.8 | 120.02 | - | - | - |

**Table 3.** Comparison of experimental and calculated bond angles of DCAP crystal.

Here the semicarbazone segment is positioned in one plane whereas acetophenone is placed perpendicular to that plane. This is the main reason for the existence of various lobe interactions which has stipulated the optical momentum [17]. The bond angle in C6-C7-N1 is found to be 114.76º between chain and ring. This is almost the semicircle angle which is making another ring spontaneously by the existence of attractive forces between ring and N-N of chain [18]. Theoretical bond angle value of H1–N3–H2 is 120.36° which is smaller than the experimental value 131o due to electronegativity of N atom. In N1-N2-H1, the theoretical bond angle is smaller than the experimental bond angle because in experimental work molecular interactions influence the electronegativity of N. Another reason for the deviation is, in experimental work a group of molecules is taken whereas in theoretical work only one molecule is taken for study hence the bond angle is affected.

## Hydrogen bonding

Hydrogen bonds are the non-covalent interactions controlling the spatial structures and their assemblies. Both intra and intermolecular hydrogen bonds (H-bonds) play a crucial role in controlling the structure of molecules as well as their functions [19]. By knowing the bond length, the strength of the hydrogen bond can be confirmed as very strong (below 2.5 Å), strong (2.5-2.7 Å), moderate (2.7-2.9 Å) and weak (above 2.9 Å). The hydrogen bonding donar-acceptor geometry is found in Table 4. It shows that both strong and weak hydrogen bonding exists.

| D-H...A | d(D-H) Å | d(H...A)Å | d(D...A)Å | <(D-H...A)deg |
|---|---|---|---|---|
| N2-H1N2...O1 | 0.85 | 2.07 | 2.907 | 168 |
| N3-H2N3...O1 | 0.81 | 2.13 | 2.924 | 164 |
| C9-H9A…O1 | 0.96 | 2.59 | 3.465 | 152 |

**Table 4.** Hydrogen bonds of DCAP (Å and °).

## Hirshfeld surface and finger print plot analysis

Hirshfeld surface analysis has recently become a popular method for the analysis of X-ray structures to investigate detailed aspects of molecular packing; for instance: polymorphism, solvatomorphism and other aspects of supramolecular arrangement. This is due to its complementary character to traditional structure viewing, where interactions are not examined in isolation but rather within the context of the whole system. Additionally, isosurface mapping is shown in Figure 6. which allows for intuitive recognition and visual analysis of interactions between the molecules. Their contributions can be expressed in terms of a percentage share. Crystal structures are imported from CIF files. Globally, the H…H contacts are the most encountered interactions in the title compound and their relative contribution reaches 26.7% followed by interactions between H…Cl about 17.3%. The next highest interactions between O…H is contributing 6.8%. The partial fingerprint plots of the title compound show that the N…H intermolecular interactions appear at the upper portion of the plot contributing 3.2% of the interactions as shown in Figure 7.

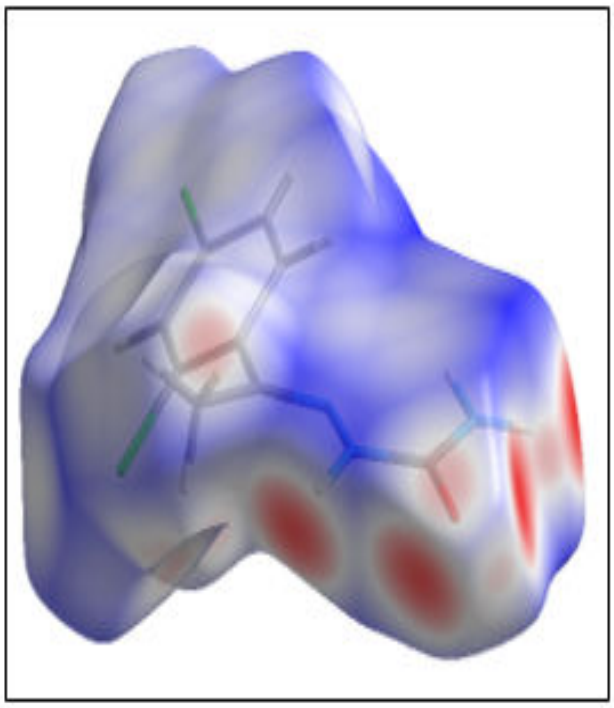

**Figure 6.** Hirshfeld surface mapped with dnorm.

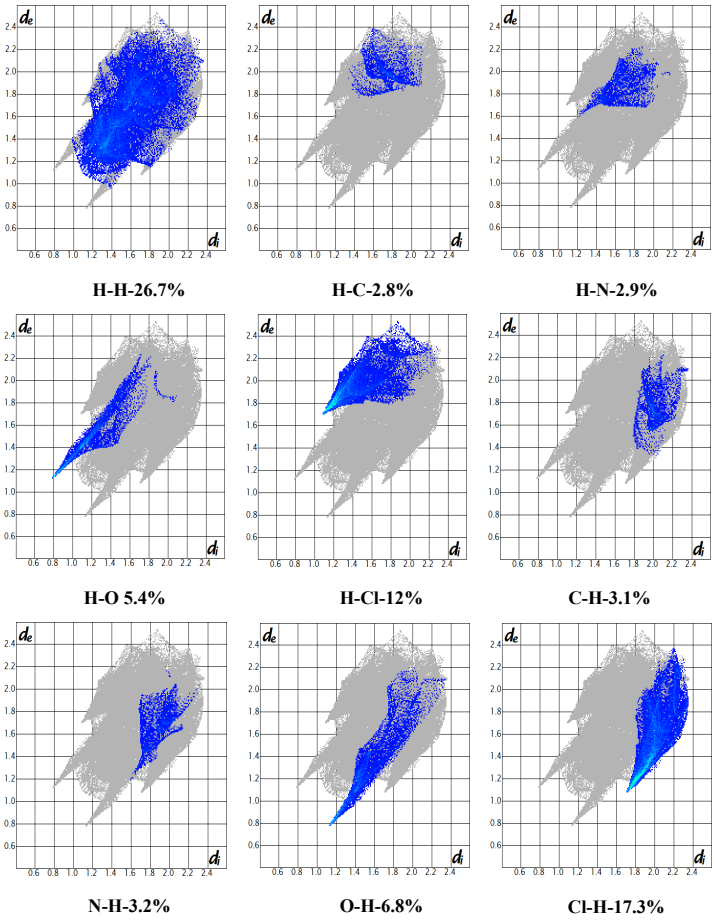


**Figure 7.** Fingerprint plots of DCAP.

## Vibrational analysis

The vibrational analysis of the grown crystal has been analyzed by FTIR and FT-Raman spectra. The present molecule DCAP consists of 24 atoms and has 66 normal modes. The title molecule belongs to C1 point group. Figure 8 and Figure 9. represent the experimental and theoretical FTIR and FT-Raman spectrum respectively. The IR and Raman scattering activities and potential energy distributions are gathered in Table 5. The realistic fundamental modes are assigned and verified along with the characteristic region of group frequencies. The entire observed modes were influenced by their nearby attractive vibrations. The molecule possesses -I effect due to the presents of chlorine in the ring. This -I effect promotes change in stretching frequencies. The carbonyl group is most important in IR spectrum because of its strong intensity absorption and high sensitivity towards minor changes in its environment. Intra and intermolecular factors affect the carbonyl absorption in common organic compounds due to inductive effect, field effect and conjugation effects.

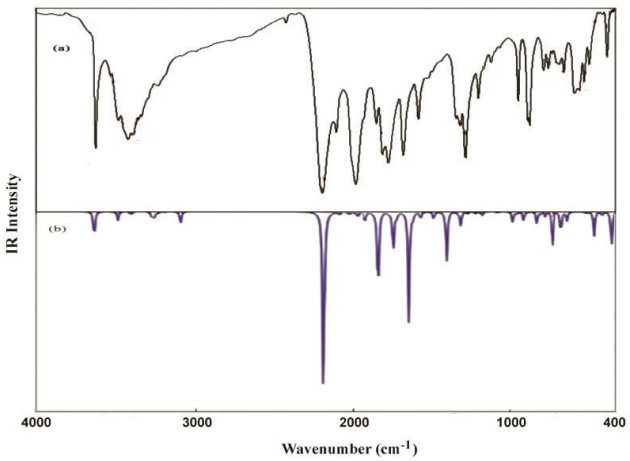


**Figure 8.** Experimental (a) and calculated (b) FTIR spectra of DCAP.

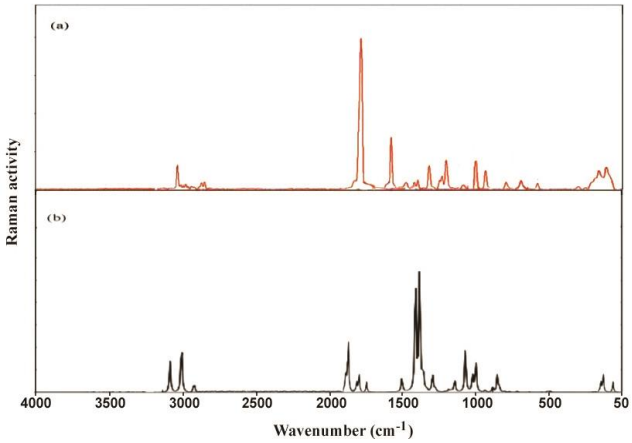


**Figure 9.** Experimental (a) and calculated (b) FT-Raman spectra of DCAP.

| S. no | Observed frequencies ($cm^{-1}$) | | Calculated frequencies with B3LYP/6-31+G(d,p) ($cm^{-1}$) | | | | % Potential Energy Distribution (PED) |
|---|---|---|---|---|---|---|---|
| | Infrared | Raman | Unscaled frequency | Scaled frequency | IR intensity | Raman activity | |
| 1 | - | - | 3755 | 3590 | 117.525 | 49.5415 | νNH (98) |
| 2 | 3477 | - | 3607 | 3448 | 36.9419 | 137.6486 | νNH (98) |
| 3 | - | - | 3569 | 3412 | 19.0726 | 168.3906 | νNH (100) |
| 4 | 3094 | - | 3235 | 3092 | 0.5677 | 77.7017 | νCH (99) |
| 5 | 3068 | - | 3225 | 3083 | 1.2995 | 141.6231 | νCH (94) |
| 6 | - | 3060 | 3195 | 3053 | 5.3664 | 63.647 | νCH (93) |
| 7 | - | - | 3154 | 3014 | 7.4766 | 42.1849 | νCH (92) |
| 8 | 2917 | 2944 | 3072 | 2936 | 9.677 | 62.7728 | νCH (100) |
| 9 | - | 2884 | 3021 | 2888 | 11.6327 | 155.5544 | νCH (92) |
| 10 | 1734 | - | 1787 | 1708 | 683.3271 | 83.6694 | νCO (77) |
| 11 | 1671 | - | 1673 | 1659 | 64.3335 | 543.9917 | νCN (78) |
| 12 | 1586 | 1583 | 1630 | 1558 | 41.5998 | 491.3892 | νCC (55), βHCC (11) |
| 13 | -- | - | 1598 | 1527 | 305.742 | 14.0259 | βHNH (84) |
| 14 | - | 1478 | 1590 | 1520 | 12.1576 | 51.3437 | νCC (54), βCCH (21) |
| 15 | 1468 | - | 1520 | 1453 | 11.6125 | 25.8963 | βHNH (10), βHCC (40) |
| 16 | 1442 | 1440 | 1501 | 1434 | 61.7474 | 33.1799 | βCH3 (57), βCNH (20) |
| 17 | - | - | 1495 | 1429 | 14.9989 | 12.188 | βHCH (65), $\beta CH_3$ (19), βCNH (11) |
| 18 | 1375 | - | 1460 | 1395 | 207.3548 | 5.3104 | βHNH (36), βHCC (18), νCC (10) |
| 19 | 1348 | - | 1413 | 1350 | 77.8313 | 10.6641 | βHCH (70), νCN (11) |
| 20 | 1343 | - | 1409 | 1347 | 179.7295 | 0.8172 | νCN (50), νCC (17), βCH (14) |

| | | | | | | | |
|---|---|---|---|---|---|---|---|
| 21 | 1338 | - | 1403 | 1340 | 61.7364 | 17.7427 | νCC (41), βHCC (12), βring (12) |
| 22 | - | 1290 | 1332 | 1273 | 53.9048 | 185.6611 | νCC (45), βCH (31), βNNH (20) |
| 23 | - | - | 1302 | 1244 | 8.7886 | 42.7899 | νCC (66), βCNN (20), βNNH (12) |
| 24 | - | - | 1280 | 1223 | 9.3764 | 2.2886 | νCC (11), βHCC (62) |
| 25 | 1142 | 1150 | 1190 | 1138 | 130.8489 | 33.514 | νNN (49), βHCC (11), βHNN (10) |
| 26 | 1110 | - | 1165 | 1113 | 130.8489 | 33.514 | βHCC (46), νNN (12), νCC (12) |
| 27 | - | - | 1123 | 1073 | 70.0514 | 18.5043 | νCC (50), βCH (23), βring (15) |
| 28 | - | - | 1118 | 1068 | 14.423 | 45.3213 | βring (19), βCNN (14) |
| 29 | 1042 | - | 1092 | 1044 | 21.087 | 5.206 | βHNC (46), νCN (27), βCH (11) |
| 30 | - | 1007 | 1054 | 1006 | 35.9343 | 14.1753 | βCCC (35), βring (18) |
| 31 | 982 | 973 | 1039 | 993 | 0.3619 | 16.0917 | δHCHC (65), dHCCC (17) |
| 32 | 947 | - | 998 | 953 | 28.5339 | 2.2908 | νCN (28), βNNH, βCH3 (14) |
| 33 | - | - | 980 | 936 | 4.8715 | 5.2146 | νCN (51), βNNC (18), βNNH, νCC (14) |
| 34 | - | - | 966 | 923 | 0.5 | 0.3473 | δNH2 (78) |
| 35 | 866 | | 887 | 848 | 13.2568 | 0.4898 | δHXXX (82) |
| 36 | - | 794 | 833 | 795 | 33.2132 | 2.6126 | δNH2 (78) |
| 37 | 754 | | 824 | 787 | 38.0189 | 4.0173 | νC-Cl (22), βCCC (33) |
| 38 | 716 | 715 | 748 | 715 | 10.5584 | 0.2299 | τOCNN (88) |
| 39 | - | - | 733 | 700 | 15.4701 | 6.1499 | δCCNC (36), τCCCC (15) |
| 40 | 686 | - | 721 | 688 | 30.9463 | 1.9388 | νC-Cl (11), δCCNC (11) |
| 41 | - | - | 677 | 647 | 4.92 | 9.2193 | βring (50), νC-Cl (11) |
| 42 | 597 | - | 612 | 584 | 13.2061 | 0.6681 | βCNN (26), βCCN (16) |
| 43 | 574 | - | 595 | 568 | 4.141 | 1.8536 | τHNCN (26), δCCNC (18), τHNNC (10) |
| 44 | 551 | - | 584 | 558 | 8.734 | 4.5065 | τHNCN (37), τCCCC (10) |
| 45 | - | 545 | 561 | 535 | 10.6412 | 1.0841 | βOCN (27), βCNH |
| 46 | - | - | 551 | 526 | 4.2117 | 4.1421 | βNCN (19), βOCN (15), βCNN (14) |
| 47 | 473 | - | 498 | 476 | 1.1187 | 0.8017 | βCCN (42), βNCO (15) |

| | | | | | | | |
|---|---|---|---|---|---|---|---|
| 48 | - | - | 470 | 448 | 10.2315 | 4.4482 | βCCC (16), βOCN (13) |
| 49 | - | - | 464 | 444 | 5.6685 | 10.5021 | δCCCC (49) |
| 50 | - | - | 438 | 419 | 111.7621 | 1.1361 | τHNNC (73) |
| 51 | - | - | 401 | 383 | 3.3861 | 8.0247 | βring (48), βCCCl (22), βCCC (16) |
| 52 | - | - | 389 | 371 | 17.8947 | 1.8805 | δCCCC (50) |
| 53 | - | - | 326 | 311 | 1.9722 | 2.2509 | βCCCl (38), βNNC |
| 54 | - | - | 292 | 279 | 9.7493 | 1.962 | βCNN (71) |
| 55 | - | 264 | 264 | 251 | 3.8807 | 2.5274 | βCCC (22), νC-Cl (10), βCC (11) |
| 56 | - | - | 244 | 233 | 169.671 | 3.9858 | τHNCN (80) |
| 57 | - | - | 222 | 212 | 11.961 | 1.2683 | δring (38) |
| 58 | - | - | 197 | 188 | 0.4356 | 1.6398 | βCCCl (76) |
| 59 | - | - | 175 | 167 | 1.4958 | 1.1108 | τCCC (47), τHCCC (16) |
| 60 | - | - | 163 | 156 | 1.5821 | 1.5836 | τHCCC (43), τCCC (21) |
| 61 | - | 124 | 138 | 132 | 2.7087 | 1.7506 | τHCCC (29), δCCN (15), δCCC (12) |
| 62 | - | 89 | 100 | 95 | 1.7314 | 0.1941 | τNNCN (17), δ CCN (16), τCCC (11), δCCCC (10) |
| 63 | - | - | 94 | 90 | 0.7688 | 6.2375 | δCCNC (77), $\delta NH_2$ (10) |
| 64 | - | - | 50 | 48 | 1.3243 | 2.0361 | δCNN (35), δCCC (11) |
| 65 | - | - | 42 | 39 | 0.4282 | 1.3385 | δCCCC (53), τNNCN (21) |
| 66 | - | - | 24 | 22 | 0.0159 | 5.7429 | τCNNC (75) |

**Note:** ν-stretching, δ-out-of-plane bending, β-in-plane bending, τ-torsion

**Table 5.** Observed and calculated frequencies of DCAP.

## C-H vibrations

In accordance with literature, the bands observed at 3094 $cm^{-1}$ and 3068 $cm^{-1}$ in IR and 3060 $cm^{-1}$ in Raman are attributed to C-H stretching. The theoretical values at 3092 $cm^{-1}$, 3083 $cm^{-1}$ and 3053 $cm^{-1}$, are assigned as C-H stretching vibrations. The peaks in IR at 1348 $cm^{-1}$ and 1110 $cm^{-1}$ is due to C-H in-plane bending vibrations. Whereas the C-H out-of-plane bending vibrations are observed at 866 $cm^{-1}$ and 982 $cm^{-1}$ in IR. Its counterpart in Raman spectrum, the peak observed at 973 $cm^{-1}$. The theoretically computed wavenumbers are in good agreement with experimental results.

## Methyl vibrations

The antisymmetric and symmetric C-H vibrations in methyl group are observed between 2920-2990 $cm^{-1}$ and 2840-2900 $cm^{-1}$. Being in excellent agreement with literature, the peaks at 2944 $cm^{-1}$, 2917 $cm^{-1}$ and 2884 $cm^{-1}$ in IR and Raman respectively, are due to antisymmetric stretching and not affected by other vibrations. The in-plane and out-of-plane vibrations are observed in the region 1340-1485 $cm^{-1}$ and 870-630 $cm^{-1}$ respectively. The peak at 1442 $cm^{-1}$ in IR and 1440 $cm^{-1}$ in Raman is due to in-plane-bending and 982 $cm^{-1}$, 973 $cm^{-1}$ are due to out-of-plane bending. The active modes of vibrational energy levels of methyl group ensured its energetic presence in the compound.

## C=O vibrations

The C=O stretching vibrations in amides occur usually around 1650-1670 $cm^{-1}$. In the present compound, the peak appeared at 1734 $cm^{-1}$ is assigned as C=O stretching vibration. The peak at 1708 $cm^{-1}$ in theoretical scaled region is in close agreement with experimental one. Due to hydrogen bonding interactions and inductive effect, the wavenumber is shifted to higher value.

## C-Cl vibrations

For the substituted benzene the C-X vibrations are shifted to lower wavenumber due to inductive or mesomeric effect of the substituents. The C-Cl stretching frequency appears in the region 600-800 $cm^{-1}$ for benzene containing Cl atom. The peaks appeared at 754 $cm^{-1}$ and 686 $cm^{-1}$ in IR are assigned for C-Cl stretching vibrations. The calculated

frequency is found at 688 $cm^{-1}$ and 787 $cm^{-1}$ which coincides with experimental ones. All these vibrational values are well within literature is mainly due to the consistent position of chlorine.

## Ring vibrations

The C–C stretching vibrations occur in the region 1625-1430 $cm^{-1}$. In the title compound, the peaks observed at 1338 $cm^{-1}$ in IR and 1586 $cm^{-1}$ and 1290 $cm^{-1}$ in Raman confirm the C-C stretching vibrations. The simulated frequencies are found to be in the expected range. The frequencies correspond to in-plane and out-of-plane bending vibrations are occurred in the expected range and coincide with literature values. Due to the extent of mixing between the ring and substituent group molecule, the wavenumbers are changed.

## C=N, C-N vibrations

The heteronuclear bond named as dipole bond (C=N, C-N) which exists with azine and methyl group. Generally, the C=N stretching vibration is observed at 1600-1490 $cm^{-1}$. In the present case, it is shifted to higher energy wavenumber at 1671 $cm^{-1}$ level due to the manifestation of Schiff base from the precursor. Another evidence for the dipole bond is C-N, which is generally observed at 1382-1266 $cm^{-1}$. In DCAP, the bands at 1343 $cm^{-1}$ and 947 $cm^{-1}$ are assigned for C-N stretching in IR. The peak is shifted is lower value due to both molecular interactions. The stimulated counterparts also coincide with literature values.

## N-N vibrations

The homonuclear bond N-N which is very important core bond of azine group acts as bridge point for NLO properties. Generally N-N stretching is observed around 1080 $cm^{-1}$. In the present case, it has overlapped with C-H bending group in IR and eluded in Raman and shifted to higher value due to the effect of bridge formation. The peak appeared at 1142 $cm^{-1}$ in IR and 1150 $cm^{-1}$ in Raman are assigned as N-N stretching. Molecular interaction is mainly concentrated between N and H in Schiff's base group of compounds.

## N-H vibration

Generally the N-H stretching vibrations occur in the region 3400-3500 $cm^{-1}$. In the present work, the peak at 3477 $cm^{-1}$ is observed for $NH_2$ stretching in IR spectrum. Theoretically, the wavenumbers at 3590 $cm^{-1}$, 3448 $cm^{-1}$ and 3412 $cm^{-1}$ are due to N–$H_2$ stretching. The N–H bending region is generally around at 1650-1580 $cm^{-1}$ and 650-895 $cm^{-1}$ for in-plane and out-of-plane bending vibrations respectively. The wave numbers at 1468 $cm^{-1}$ and 1375 $cm^{-1}$ in IR attribute to N-H bending and the peak at 794 $cm^{-1}$ is $NH_2$ deformation vibration. Theoretical counterparts are also observed in the expected region.

## VCD spectrum

Vibrational Circular Dichroism (VCD) is an electro-magneto-optic effect and associated with spectroscopic technique which detects differences in attenuation of left and right circularly polarized light passing through the compound [18]. VCD is the coupling of optical activity to infrared vibrational spectroscopy. More specifically, the essence of VCD is to combine the stereo chemical sensitivity of natural optical activity with the rich structural content of vibrational spectroscopy. The result of a VCD measurement is the combination of two vibrational spectra; VCD and its parent infrared spectrum. These can be used together to deduce information regarding elucidation of optically and biologically significant molecules. The VCD spectrum of the present molecule is depicted in Figure 10.

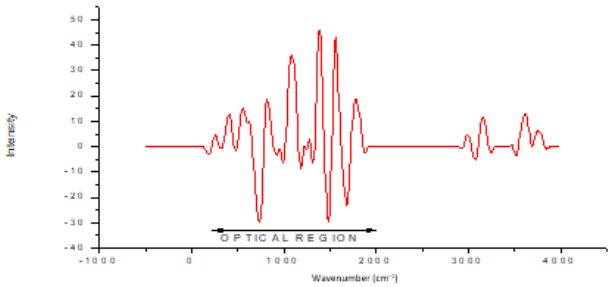


**Figure 10.** VCD spectrum of DCAP.

In the present molecule the spectrum originated from zero and the intensity of the absorption is elevated in positive and negative sides due to the left and right circular polarization. The vibrational polarization bands belong to middle IR region which corresponds to the C=N, C=C, C=O, C-C, N-N and C-N stretching vibrations and N-H and C-H in-plane bending wavenumbers. All such vibrational bands stated that, the functional groups are active and eventually confirms the non-linearity [19,20].

## UV-visible-NIR spectral analysis

The optical absorption spectrum is used to study the band structure and the kind of electronic transition occurring in the analysed sample. The maximum absorbance at 215 nm corresponds to $\pi \rightarrow \pi^*$ transition which is due to the conjugation of semicarbazone group with the acetoketone group. The band gap energy is found to be 5.78 eV. The band gap energy also ensures that the grown crystal possess dielectric behaviour to induce the polarization when the powerful radiation is incident on the material. The calculated maximum wavelength at 287 nm is correlated with experimental $\lambda_{max}$ and the excitation energy is calculated to be 5.78 eV. The transitions are active in the UV-vis region signifying the NLO activity. The UV-visible-NIR spectrum studied experimentally and theoretically is exhibited in Figures 11a-c. Table 6 contains both experimental and theoretical values and its major contribution with oscillator strength.

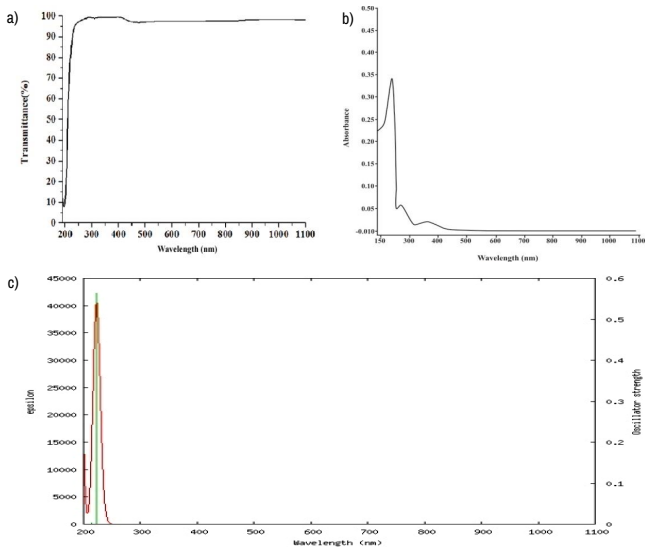


**Figure 11.** a) UV-Vis-NIR transmittance spectrum of DCAP, b) UV-Vis-NIR absorption spectrum of DCAP, c)Theoretical UV-Vis spectrum of DCAP

| Excited state | Wavelength(λ) nm | | Excitation Energies (eV) | Oscillator strength (f) | Major contribution | Assignment |
|---|---|---|---|---|---|---|
| | Theoretical | Experimental | | | | |
| S1 | 222.79 | - | 4.4884 | 0.5637 | H → L+2 (35%) | π→π* |
| S2 | 213.12 | 215 | 4.6921 | 0.0021 | H → L (98%) | π→π* |
| S3 | 192.04 | - | 5.2071 | 0.8707 | H → L+1 (96%) | π→π* |

**Table 6.** Experimental and theoretical electronic absorption spectral values of DCAP.

## Photoluminescence spectral analysis

Photoluminescence is one of the effective tools to provide information about the various energy levels due to excitation energy. The photoluminescence emission spectrum of DCAP is recorded with an excitation wavelength of 215 nm. It is found that the wavelength of DCAP is red shifted to 618 nm indicating the fact that the crystal can also be used for IR applications. It is noted that during emission, an increase in intensity of DCAP spectrum shows hyperchromic shift which is shown in Figure 12.

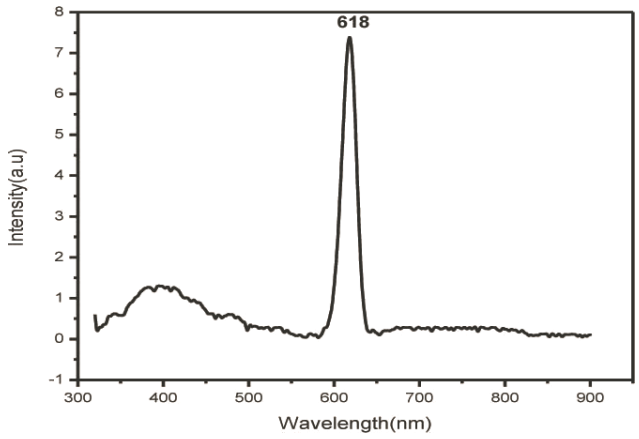


**Figure 12.** Photoluminescence emission spectrum of DCAP.

## Electrical properties

The variation of dielectric constant as a function of frequency at room temperature is shown in Figure 13a. The high value of dielectric constant at low frequencies may be due to the presence of electronic, ionic dipolar and space charge polarizations and its low value of higher frequencies may be due to loss of these polarizations gradually. According to the Miller's rule lower value of dielectric constant is one of the suitable properties for the enhancement of SHG co-efficient. The dielectric loss is studied as a function of frequency at room temperature which is shown in Figure 13b. The minimum value of dielectric loss at high frequency indicates the enhanced optical quality of the crystal with lesser defects.

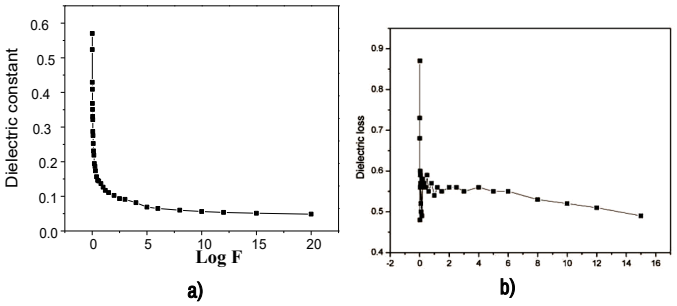


**Figure 13.** Variation of dielectric constant and loss with Log F of DCAP.

## Second harmonic generation efficiency

The SHG relative efficiency for the title crystal measured by Kurtz's Perry powder technique which generates the second harmonic output by irradiating the powder samples of randomly oriented crystallites. The powdered sample sandwiched between two glass slides is subjected to the output of a Q-Switched Nd:YAG laser emitting a fundamental wavelength of 1064 nm. The SHG efficiency is confirmed by the emission of green radiation (532 nm). The laser with input voltage 0.68mJ is given as input. The output voltage for urea and DCAP is 8.9 mJ and 3.67 mJ respectively. The SHG efficiency is compared with urea and it is found to be 0.4 times greater than that of urea crystal.

## Thermal analysis

Thermogravimetric methods are largely limited to decomposition and oxidation reactions which are physical processes such as vaporization and sublimation. Thermograms provide information about decomposition patterns of materials and also weight loss. Figure 14 shows the differential thermogram of DCAP crystal. The analysis is performed between 25°C and 1400°C at a heating rate of 101°C/min in the nitrogen atmosphere. There is only one stage of weight loss noted in the thermogram. The sharp endothermic peak is observed at 249°C which shows that the compound is thermally stable up to 249°C.

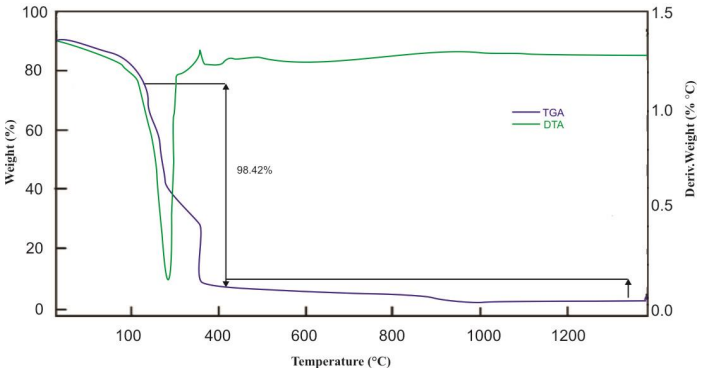


**Figure 14 .**TG/DTA curves of DCAP.

## Theoretical first order hyperpolarzibility

The first-order hyperpolarizability (β) is the second-order electric susceptibility per unit volume. The molecules exhibiting large hyperpolarizabilities have a strong NLO Potential and could be useful for optical devices. For exhibiting larger molecular hyperpolarizabilities, the system must be asymmetric and should contain polarizable electron donor and acceptor groups. The calculated magnitudes of second order polarizability, dipole moment and polarizibility for the DCAP crystal are shown in Table 7. The results authenticate that the grown crystal is 13.35 times greater than that of standard urea hence it can be used for non-linear applications.

| Parameters | Dipole moment (Debye) | Parameters | Polarizability (a.u) | Parameters | Hyperpolarizabiltiy (a.u) |
|---|---|---|---|---|---|
| μx | -1.87 | $\alpha_{xx}$ | 254.12 | $\beta_{xxx}$ | -470.88 |
| μy | 0.24 | $\alpha_{xy}$ | -9.42 | $\beta_{xxy}$ | 29.52 |
| μz | -0.03 | $\alpha_{yy}$ | 151.72 | $\beta_{xyy}$ | -7.13 |
| μ | 1.89 | $\alpha_{xz}$ | -9.96 | $\beta_{yyy}$ | -112.63 |
| - | - | $\alpha_{yz}$ | -10.21 | $\beta_{xxz}$ | 5.75 |
| - | - | $\alpha_{zz}$ | 106.75 | $\beta_{xyz}$ | 77.26 |
| - | - | $\alpha_{tot}$ | 170.86 | $\beta_{yyz}$ | -26.3 |
| - | - | $\alpha_{tot}$esu | 25.32 x $10^{-24}$ esu | $\beta_{xzz}$ | -40.62 |
| - | - | - | - | $\beta_{yzz}$ | -26.93 |
| - | - | - | - | $\beta_{zzz}$ | 39.57 |
| - | - | - | - | $\beta_{tot}$ | 13.35 x $10^{-30}$ esu |

**Table 7.** Dipole moment (μ), polarizability and first-order hyperpolarizability (β) of DCAP derived from DFT calculation at 6-31+G(d,p) basis set.

## Frontier molecular orbital analysis

The frontier orbital's (HOMO and LUMO) find out the way in which the molecule interacts with other species. The frontier orbital gap facilitates to characterize the chemical reactivity and kinetic stability of the molecule. A molecule with a small frontier orbital gap is more polarizable and is usually related with a high chemical reactivity, low kinetic stability and is also termed as soft molecule. Highest Occupied Molecular Orbital (HOMO) is directly related to the ionization potential, while energy of the Lowest Unoccupied Molecular Orbital (LUMO) is directly related to the electron affinity. The HOMO is the orbital that primarily acts as an electron donor and the LUMO is the orbital that mainly acts as the electron acceptor. It can be seen from the Figure 15. HOMO of DCAP presents a charge density localized over the benzene ring LUMO is characterized by a charge distribution on the entire molecule except of hydrogen atoms in CH3 group. The HOMO and LUMO transition implies an electron density transfer. Moreover, lower in the HOMO and LUMO energy gap explains the eventual charge transfer interactions taking place within the molecule. Usually, the chemical applications would be extracted from the chemical properties of the compounds. They can also be useful for identifying new substance for the particular purpose. It is very important to know whether this compound is suitable for optical application. In this way, the ionization potential, electron affinity, electronegativity, chemical hardness and electrophilicity index are tabulated in Table 8. The chemical hardness of the present compound is 2.4152 eV. Therefore, the present compound has much chemical stability. Here, the substitutions of semicarbazone group have enhanced the chemical stability and rigidity character of the DCAP. So, in the present compound, the optical property has been tuned on the timescale of its expected NLO utility.

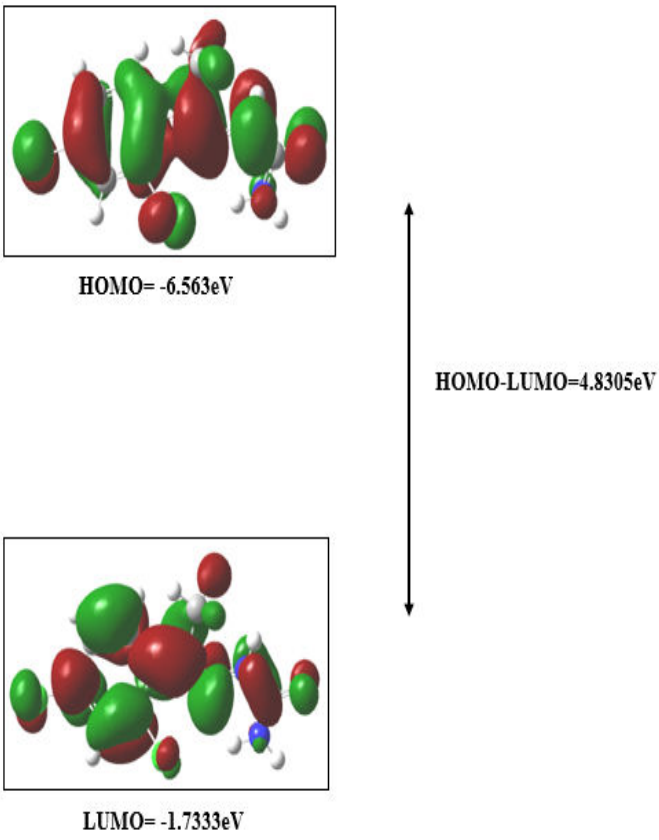


**Figure 15.** Frontier molecular orbitals of DCAP.

| Parameters | DCAP |
|---|---|
| $E_{HOMO}$ | -6.5638 eV |
| $E_{LUMO}$ | -1.7333 eV |
| $E_{HOMO}$-$E_{LUMO}$ | 4.8305 eV |
| Ionisation potential | 6.5638 eV |
| Electron affinity | 1.7333 eV |
| Chemical hardness($\eta$) | 2.41522 eV |
| Softness ($\zeta$) | 0.4140 eV |
| Electronegativity ($\chi$) | 4.1485 eV |
| Electrophilicity index ($\psi$) | 20.7850 eV |

**Table 8.** Calculated molecular orbital parameters of DCAP employing 6-31+G(d,p) basis set.

The electronegativity is a chemical property which describes the tendency of a molecule or a functional group to attract electrons (or electron density) towards itself. If the compound possesses high electronegativity number, the compound will have the high degree of electron density. Usually, the accumulation of electron density is associated more with different functional groups than with individual atoms called group electronegativity. In this compound, the group electronegativity is found to be 4.148 eV which is high and the property of chemical bonds in the title molecule is virtually ionic. Accordingly, due to the combination of two groups of atoms, the bonds character of the compound reformed to be ionic.

## Molecular electrostatic potential surface

The Molecular Electrostatic Surface Potential (MESP) is a technique of mapping electrostatic potential onto the iso-electron density

surface. The importance of MEP is originated from it from it simultaneously displays molecular size, shape as well as positive, negative and neutral electrostatic potential regions in terms of color grading. In other words, electrostatic potential increases in the order red<orange<yellow<green<blue. The negative region is localised on oxygen and slightly electron deficient on N-N. A maximum positive region is localized over another side of $CH_3$ group indicating a probable site for nucleophilic aggression. From these results, it is clear that, the semicarbazone group is the main root cause of active NLO properties of the compound. The predominance of light green region resides on the aromatic ring. MESP map of DCAP is shown in Figure 16.

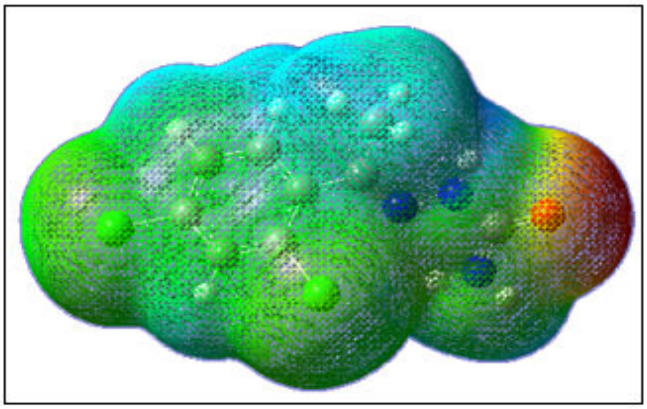

**Figure 16.** MESP of DCAP.

## Conclusion

In order to confirm the NLO responses of the present compound both experimental characterizations and theoretical calculations are carried out. The SXRD confirms that the structure belongs to monoclinic system. FTIR and FT-Raman spectra confirm the functional groups present in DCAP. The optical properties like UV-vis, PL, SHG confirm its nonlinearity. Dielectric constant and dielecric loss confirm the polarization nature of DCAP. The crystal belongs to soft material category which is confirmed by Vickers hardness test. The theoretical investigations like vibrational analysis, HOMO-LUMO, ESP, VCD spectrum and hyperpolarizibility calculations evaluate that the compound has dynamic NLO property. The Hirshfeld analysis shows the strong interactions present in the compound. The obtained results were coherent and the entire analysis explored the presence of NLO activity present in the compound. Therefore, the DCAP crystal is very interesting material for optical applications due to its Nonlinear property.

## References


1. Williams, David J. "Nonlinear Optical Properties of Organic and Polymeric Materials." *J Am Chem Soc* 1983.
2. Zyss, Jnl. "Nonlinear Organic Materials for Integrated Optics-A Review." *J Mol Electron* 1 (1985): 25-45.
3. Maloney, C and W. Blau. "Resonant Third-Order Hyper Polarizabilities of Large Organic Molecules." *JOSA B* 4 (1987): 1035-1039.
4. Garito, A. F, C. C. Teng, K. Y. Wong and O. Zammani'Khamiri. "Molecular Optics: Nonlinear Optical Processes in Organic and Polymer Crystals." *Mol Cryst Liq Cryst* 106 (1984): 219-258.
5. Li, Zhengdong, Baichang Wu and Genbo Su. "Nonlinear-Optical, Optical and Crystallographic Properties of Methyl P-Hydroxybenzoate." *J Cryst Growth* 178 (1997): 539-544.
6. Hidalgo-Lopez, A. and S. Veintemillas-Verdaguer. "Growth of $K_2Mg_2(SO_4)_3$ and $K_2Mn_2(SO_4)_3$ from Solution By Solvent Evaporation and Diffusion-Reaction Methods." *J Cryst Growth* 178 (1997): 559-567.
7. Lee, Chengteh, Weitao Yang and Robert G. Parr. "Development of the Colle-Salvetti Correlation-Energy Formula into a Functional of the Electron Density." *Phys Rev B Condens Matter* 37 (1988): 785.
8. Fogarasi, Geza, Xuefeng Zhou, Patterson W. Taylor and Peter Pulay. "The Calculation Of Ab Initio Molecular Geometries: Efficient Optimization By Natural Internal Coordinates and Empirical Correction By Offset Forces." *J Am Chem Soc* 114 (1992): 8191-8201.
9. Fun, H-K., Chin Sing Yeap, Shridhar Malladi and Mahesh Padaki et al. "2-(4-Methylanilino) Acetohydrazide." *Acta Crystallogr Sect E Struct Reports Online* 65 (2009): 2234-2234.
10. Lind, Per. "Organic and Organometallic Compounds for Nonlinear Absorption of Light." 2007.
11. Moorthy, N., P. Jobe Prabakar, S. Ramalingam and S. Periandy, et al. "Spectroscopic Investigation of The Stimulus of NLO Property On Acetone Thiosemicarbazone Using Computational (HF And DFT) Confinement." *J Theor Comput Sci* 2 (2015): 2.
12. Moorthy, N., PC Jobe Prabakar, S. Ramalingam and G. V. Pandian, et al. "Vibrational, NMR and UV–Visible Spectroscopic Investigation and NLO Studies on Benzaldehyde Thiosemicarbazone Using Computational Calculations." *J Phys Chem Solids* 91 (2016): 55-68.
13. Patai, Saul. "The chemistry of the carbonyl group." (1966).
14. Savithiri, S, G. Rajarajan, V. Thanikachalam and S. Bharanidharan, et al. "Spectroscopic (FT-IR, FT-Raman) and Quantum Mechanical Studies of 3t-Pentyl-2r, 6c-Diphenylpiperidin-4-One Thiosemicarbazone." *Spectrochim Acta A Mol Biomol Spectrosc* 136 (2015): 782-792.
15. Moorthy, N., PC Jobe Prabakar, S. Ramalingam and M. Govindarajan, et al. "Spectroscopic Analysis, AIM, NLO and VCD Investigations of Acetaldehyde Thiosemicarbazone Using Quantum Mechanical Simulations." *J Phys Chem Solids* 95 (2016): 74-88.
16. Moorthy, N., PC Jobe Prabakar, S. Ramalingam and S. Periandy, et al. "Vibrational, NMR and UV-Visible Spectroscopic Investigation, VCD and NLO Studies On Benzophenone Thiosemicarbazone Using Computational Calculations." *J Mol Struct* 1110 (2016): 162-179.
17. Senes, Alessandro, Iban Ubarretxena-Belandia and Donald M. Engelman. "The Cα-H... O Hydrogen Bond: A Determinant Of Stability AND Specificity in Transmembrane Helix Interactions." *Proc Natl Acad Sci* 98, (2001): 9056-9061.
18. Nikolaienko, Tymofii Yu, Leonid A. Bulavin and Dmytro M. Hovorun. "Bridging QTAIM with Vibrational Spectroscopy: The Energy of Intramolecular Hydrogen Bonds in DNA-Related Biomolecules." *Phys Chem Chem Phys* 14 (2012): 7441-7447.
19. Karthikeyan, N., J. Joseph Prince, S. Ramalingam and S. Periandy. "Spectroscopic (FT-IR And FT-Raman) and Theoretical (UV–Visible And NMR) Analysis on A-Methylstyrene By DFT Calculations." *Spectrochim Acta A Mol Biomol Spectrosc* 143 (2015): 107-119.
20. Pearson, Ralph G. "Absolute Electronegativity and Hardness Correlated with Molecular Orbital Theory." *Proc Natl Acad Sci* 83 (1986): 8440-8441.


**How to cite this article:** Ananthi, R. "Crystal Growth, Characterization and Theoretical Insights of an Organic Schiff base 2-(1-(2,4 Dichlorophenyl)Ethylidene)Hydrazine Carboxamide for NLO Applications." *J Laser Opt Photonics* 12 (2025): 180.